

in Figure 3 and the previous estimates based on the branching ratios.

### Conclusions

We have shown that methane loss from acetone cation does not occur by a tunneling mechanism in the IRMP dissociation.<sup>11</sup> The large isotope effects observed in this system appear to arise from competitive reaction isotope effects. Using IRMP branching ratios we were able to estimate the energy difference between methane loss and methyl loss as well as ZPVE differences associated with isotopic substitution. These estimates agree with ZPVE differences obtained with frequencies from *ab initio* calculations.

Competitive reaction isotope effects should occur in other gas phase ion reactions. A general mechanism involving ion-neutral complexes and hydrogen atom abstraction has arisen for many low-energy rearrangements<sup>12-19</sup> (eq 2). ZPVE differences due to isotopic substitution can raise the energy for the abstraction so that it is not lower in energy than the complex simply dissociating. We believe that several previous studies can be understood by considering these issues.<sup>16,30,49-52</sup>

**Acknowledgment.** We are grateful to the National Science Foundation for support of this work. We thank Professors Helmut Schwarz and Chava Lifshitz for insights and helpful discussions. We are grateful to Professor Robert McIver and Dr. Richard Hunter of IonSpec for considerable technical help. T.H.O.

(49) Holmes, J. L.; Burgers, P. C.; Mollah, M. Y. A.; Wolkoff, P. *J. Am. Chem. Soc.* **1982**, *104*, 2879.

(50) Holmes, J. L.; Burgers, P. C.; Mollah, Y. A. *Org. Mass. Spectrom.* **1982**, *17*, 127.

(51) Donchi, K. F.; Brownlee, R. T. C.; Derrick, P. J. *J. Chem. Soc., Chem. Commun.* **1980**, 1061.

(52) McAdoo, D. J.; Traeger, J. C.; Hudson, C. E.; Griffin, L. L. *J. Phys. Chem.* **1988**, *92*, 1524.

(53) Baer, S. Ph.D. Thesis, Stanford University, 1990.

(54) Osterheld, T. H. Unpublished results.

gratefully acknowledges graduate fellowship support from the W. R. Grace Foundation.

### Appendix. Estimates of Reaction Threshold Differences Using Branching Ratios from CW Laser Photolysis

We assume that the energy range goes from threshold to 2.99 kcal/mol above threshold. The energy equivalent of P(22) and P(24) photons from the 9.6- $\mu\text{m}$  transition is 2.99 kcal/mol. The range starts at threshold because methane loss should be faster than the  $10\text{-s}^{-1}$  pumping rate essentially at threshold.

We assume a square (uniform) energy distribution over the 2.99 kcal/mol range. The energy distribution after electron impact ranges from the ionization potential to the lowest energy threshold and contains resonances which are observed in the photoelectron spectrum. Under irradiation the ions undergo transitions up and down the vibrational ladder due to absorption and stimulated emission, which should help to "smear" out the resonances in the distribution. The resonances also tend to be much broader than 2.99 kcal/mol. Other experiments in our laboratory support this square energy distribution proposal.<sup>53</sup>

Given these assumptions, the difference between the methane and methyl loss thresholds comes from  $X$  in the following equation:

$$\text{branching ratio} = \frac{2.99 - X}{X} \quad (6)$$

For example, acetone cation has a branching ratio of 2.4, which gives an energy range for methane loss of 0.88 kcal/mol. Methyl loss is more facile than methane loss and should dominate at an energy slightly above the methyl loss threshold.<sup>3,5,30-32,37</sup> Equation 6 assumes that an ion will eliminate methane below the methyl loss threshold and not above. While this assumption is not strictly true, it should be reasonable because little methane loss is observed in pulsed laser photolysis at high fluences.<sup>54</sup>

Registry No.  $\text{H}_3\text{CCOCH}_3^{++}$ , 34484-11-2;  $\text{D}_2$ , 7782-39-0;  $\text{H}_2$ , 1333-74-0;  $\text{CH}_4$ , 74-82-8;  $\text{CH}_3\text{CO}^+$ , 15762-07-9;  $\text{CH}_3^+$ , 2229-07-4;  $\text{CH}_2\text{CO}^{++}$ , 64999-16-2;  $\text{D}_3\text{CCOCH}_3$ , 7379-29-5;  $\text{H}_3\text{CCHO}$ , 75-07-0;  $\text{CD}_3\text{I}$ , 865-50-9;  $\text{D}_3\text{CCH}(\text{O}^-)\text{CH}_3$ , 142465-08-5.

## The Bromite-Iodide Clock Reaction<sup>1</sup>

Roberto de Barros Faria,<sup>†</sup> Irving R. Epstein,\* and Kenneth Kustin\*

Contribution from the Department of Chemistry, Brandeis University, Box 9110, Waltham, Massachusetts 02254-9110. Received March 4, 1992

**Abstract:** Clock reaction behavior has been found in the pH range 6-8 for the reaction between bromine(III) and iodide ion when the initial bromine(III) concentration exceeds one-fourth the initial iodide ion concentration. The overall stoichiometry is  $2\text{I}^- + 3\text{HBrO}_2 \rightarrow 2\text{IO}_3^- + 3\text{Br}^- + 3\text{H}^+$ . In this relatively fast clock reaction, a brown color due to formation of  $\text{I}_2$  and  $\text{I}_3^-$  intensifies, reaches a peak, and then abruptly disappears. For total initial bromine(III) ( $[\text{Br}^{\text{III}}]_0$ ) and iodide ion ( $[\text{I}^-]_0$ ) concentrations of  $8.6 \times 10^{-4}$  and  $5 \times 10^{-4}$  M, respectively, the time to reach the peak increases from 0.23 s at pH 6 to 6 s at pH 8. After that stage of reaction,  $\text{I}_2$  is oxidized relatively rapidly according to  $2\text{I}_2 + 5\text{HBrO}_2 + 2\text{H}_2\text{O} \rightarrow 4\text{IO}_3^- + 5\text{Br}^- + 9\text{H}^+$ . A secondary, smaller increase in optical absorbance occurs when  $1/4 < [\text{Br}^{\text{III}}]_0/[\text{I}^-]_0 < 3/2$ . The rate law has been redetermined for the process  $4\text{I}^- + \text{HBrO}_2 + 3\text{H}^+ \rightarrow 2\text{I}_2 + \text{Br}^- + 2\text{H}_2\text{O}$ , which initiates the clock reaction. A mechanism incorporating autocatalytic formation of HOI, in which IBr is a transient but significant intermediate, has been developed which successfully models the system's dynamical behavior in computer simulations.

### Introduction

The kinetics of bromine(III) reactions acquired particular significance following the development of mechanisms to explain oscillations in the Belousov-Zhabotinsky (BZ) reaction wherein an organic species, e.g. malonic acid, is oxidized by bromate ion at high acidity in the presence of a catalyst such as  $\text{Ce}^{\text{III}}/\text{Ce}^{\text{IV}}$ .<sup>2</sup>

Few experimental studies of bromine(III) reactions were known, however, because this oxyhalogen was not commercially available at that time, and it is unstable below pH 6-7 where the predominant Br(III) species is bromous acid,  $\text{HBrO}_2$ . Thus, studies of

(1) Systematic Design of Chemical Oscillators. Part 81. For Part 80, see: Rábai, Gy.; Epstein, I. R. *J. Am. Chem. Soc.* **1992**, *114*, 1529.

(2) Field, R. J.; Burger, M., Eds. *Oscillations and Traveling Waves in Chemical Systems*; Wiley: New York, 1985.

<sup>†</sup> Departamento de Química Inorgânica, Instituto de Química, Universidade Federal do Rio de Janeiro, 21941 Rio de Janeiro, RJ, Brazil.

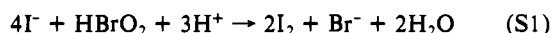
Table I. Rate Law Determination of Reaction S1

$[\text{Br}^{\text{III}}]_0$ , M	$[\text{I}^-]_0$ , M	pH	$\mu$ , M	buffer <sup>a</sup>	reagent order	$k^b$
$1 \times 10^{-3}$	$1 \times 10^{-4}$ to $3 \times 10^{-3}$	6.04	0.10	A	0.86	$8.07 \times 10^8$
$1 \times 10^{-3}$	$2.5 \times 10^{-4}$ to $8 \times 10^{-3}$	8.08	0.15	A	0.88	$8.20 \times 10^8$
$2.5 \times 10^{-4}$ to $2.5 \times 10^{-3}$	$1 \times 10^{-3}$	6.03	0.15	A	0.88	$1.49 \times 10^9$
$2.5 \times 10^{-4}$ to $5 \times 10^{-3}$	$5 \times 10^{-4}$	6.05	0.10	A	0.94	$2.12 \times 10^9$
$1 \times 10^{-3}$	$1 \times 10^{-3}$	6.03-8.09	0.15	A	1.18	$2.50 \times 10^{10}$
$2.5 \times 10^{-5}$	$1 \times 10^{-4}$	4.40-5.89	0.15	B	1.009	$1.97 \times 10^9$
$2.5 \times 10^{-5}$ to $1.5 \times 10^{-4}$	$1 \times 10^{-4}$	5.70	0.10	B	1.11	$2.89 \times 10^9$
$2.5 \times 10^{-5}$	$1 \times 10^{-4}$ to $1 \times 10^{-3}$	5.70	0.10	B	1.01	$1.11 \times 10^9$

<sup>a</sup> Buffer A =  $\text{Na}_2\text{HPO}_4 + \text{NaOH}$ ; buffer B = potassium biphthalate +  $\text{NaOH}$ . <sup>b</sup> Third-order rate constant ( $\text{M}^{-2} \text{s}^{-1}$ ) assuming 1.0 for all reagent orders.

both the decomposition kinetics of aqueous sodium bromite,<sup>3</sup> and its reactions with various inorganic substrates were carried out above pH 9.<sup>4,5</sup> A notable exception to this trend was the study of the reaction between  $\text{Br}(\text{III})$  and iodide ion in the pH range 5.5-8 under conditions of excess iodide ion concentrations.<sup>6</sup>

In this pH range, with a stoichiometric excess of iodide ion, for example, initial concentrations  $[\text{I}^-]_0 = 0.01 \text{ M}$  and  $[\text{Br}^{\text{III}}]_0 = 1.2 \times 10^{-5} \text{ M}$ , reaction S1 occurs. The authors reported a rate



law for this reaction, general acid catalysis, and a decrease in reaction rate constant with increase in ionic strength.<sup>6</sup>

In contrast to the BZ reaction, which was discovered by serendipity, a large family of oscillators has been deliberately designed by taking advantage of the autocatalytic and autoinhibitory dynamics exhibited by the  $\text{Cl}^{\text{III}}-\text{I}^-$  reaction.<sup>7</sup> The recent availability of sodium bromite from a commercial source<sup>8</sup> encouraged us to study this system with the intention of pursuing the design of chemical oscillators based on bromine(III) chemistry. We therefore report on the kinetics and mechanism of the reaction between bromine(III) and iodide ion in the pH range 4.5-8 under conditions of excess bromine(III).

### Experimental Section

**Materials.** All reagents ( $\text{NaClO}_4$ , Aldrich; all the rest, Fisher) were of the highest purity available and were used without further purification, except for  $\text{NaBrO}_2 \cdot 3\text{H}_2\text{O}$  (Aldrich).

In most experiments,  $\text{Br}(\text{III})$  solutions were prepared by dissolving the intended amount of sodium bromite trihydrate in 0.1 M  $\text{NaOH}$ , followed by additional dilution with deionized water to 0.01 M  $\text{NaOH}$ . Stock solution titer was checked every week,<sup>9</sup> and the stock solution was discarded after 1 month even if its concentration was not observed to have changed. In a typical analysis we found that the solid reagent had 86% of the bromine atoms as  $\text{BrO}_2^-$ , the remainder being present as  $\text{BrO}_3^-$  and  $\text{Br}^-$ . We did not find measurable amounts of  $\text{BrO}^-$ . The presence of  $\text{BrO}_3^-$  impurity in the reagent does not pose a problem, as reactions of  $\text{BrO}_3^-$  are too slow at pH 4.5-8 to interfere with the very rapid bromine(III) reactions.

As the supply of sodium bromite trihydrate ages, the amount of bromide increases due to decomposition. Solutions made from such a supply of  $\text{Br}(\text{III})$  showed small differences in kinetics curves from repeat experiments. Purifying this reagent restored curves to their initial aspect. A typical purification begins with dissolving 0.5 g of the solid reagent in 10 mL of deionized water (the pH in this solution is usually around 10). Upon dropwise addition of  $\text{AgNO}_3$  ( $1 \times 10^{-2} \text{ M}$ ) with stirring,  $\text{AgBr}$  precipitates. Elimination of  $\text{Br}^-$  was accompanied by  $[\text{Br}^-]$  determination with a bromide-selective electrode. The  $\text{AgNO}_3$  addition is stopped when  $[\text{Br}^-]$  is around  $1 \times 10^{-6} \text{ M}$  or less. Some  $\text{AgBr}$  is in a negatively charged colloidal state; consequently, we added barium hydroxide (usually 15 mg of the solid octahydrate) to flocculate the colloid. After this mixture was stirred for some 5 to 10 min, it was filtered with a sintered glass filter (grade "F"). The filtrate was checked for  $\text{Ba}^{2+}$  by addition of sodium sulfate solution. This test did not show any detectable barium cation, because the amount of barium salt added is small, and it is totally adsorbed by the colloidal  $\text{AgBr}$ . After addition of sodium hydroxide solu-

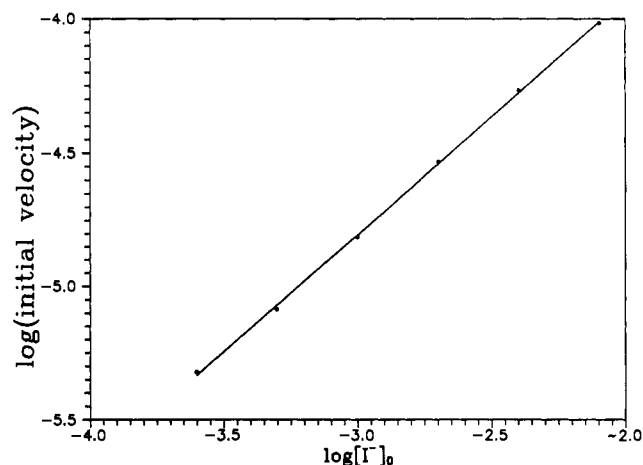


Figure 1. Determination of  $[\text{I}^-]$  order in reaction S1: 0.05 M phosphate buffer pH 8,  $[\text{Br}^{\text{III}}]_0 = 1.0 \times 10^{-3} \text{ M}$ ,  $\mu = 0.15 \text{ M}$ .

tion, this solution is diluted to the desired volume with deionized water to produce the stock sodium bromite solution in 0.01 M  $\text{NaOH}$ .

**Methods.** Reactions were carried out in 0.05 M phosphate buffer or 0.05 or 0.025 M phthalate buffer;  $\text{NaClO}_4$  was used to adjust the ionic strength,  $\mu$  (M). The pH was measured with an Orion Research pH meter, Model 801A, together with a combination pH electrode (Aldrich, Model Z11323-9). In some experiments, the 0.05 M phosphate buffer (without  $\text{NaClO}_4$ ) was present in considerable excess compared with other reagents and was primarily responsible for the ionic strength of approximately  $6 \times 10^{-2} \text{ M}$ .

Kinetics curves were determined at  $25 \pm 0.1 \text{ }^\circ\text{C}$  in a Hi-Tech SF-3L stopped-flow spectrophotometer. The iodine concentration was monitored by measuring its optical absorbance at the  $\text{I}_2/\text{I}_3^-$  isosbestic point of wavelength (nm),  $\lambda$ , equal to 470 nm and molar absorbance coefficient ( $\text{M}^{-1} \text{cm}^{-1}$ ),  $\epsilon$ , equal to  $740 \text{ M}^{-1} \text{cm}^{-1}$ .<sup>10</sup>

Transmittance curves were stored on a diskette and converted to absorbance with Lotus 1-2-3 as follows. For each experiment at least 10 curves were acquired and superimposed on one another on the screen of the computer. The traces that deviated significantly from the others were discarded. The others, usually more than five, were averaged and then converted to absorbance.

### Results

**Production of Iodine.** The homologous reaction between  $\text{Cl}(\text{III})$  and  $\text{I}^-$  is autocatalytic in iodine and autoinhibitory in iodide.<sup>11,12</sup> It therefore seemed worthwhile to reevaluate the rate law previously determined for the  $\text{Br}^{\text{III}}-\text{I}^-$  reaction, under conditions of excess  $[\text{I}^-]_0$ , in which autocatalysis is not exhibited, as we have confirmed, experimentally. We reexamined the order of the reaction with respect to  $[\text{I}^-]$ ,  $[\text{Br}^{\text{III}}]$ , and the influences of  $[\text{H}^+]$ , specific buffer, and ionic strength on the observed rate constant. These effects have been evaluated by plotting the logarithm of initial velocity against the logarithm of  $[\text{I}^-]$ ,  $[\text{Br}^{\text{III}}]$ , and  $a_{\text{H}^+}$  ( $a_{\text{H}^+}$  is hydrogen ion activity), respectively, for different buffers and ionic strengths. A representative plot is shown in Figure 1. The results have been summarized in Table I.

(3) Lee, C. L.; Lister, M. W. *Can. J. Chem.* **1971**, *49*, 2822.

(4) Lee, C. L.; Lister, M. W. *Can. J. Chem.* **1979**, *57*, 1524.

(5) Jhanji, A. K.; Gould, E. S. *Int. J. Chem. Kinet.* **1991**, *23*, 229.

(6) Ferranti, F.; Indelli, A. *Gazz. Chim. Ital.* **1972**, *102*, 117.

(7) Epstein, I. R.; Kustin, K. *Struct. Bonding* **1984**, *56*, 1.

(8) Anonymous. *Aldrichim. Acta* **1985**, *18*, 94.

(9) Hashmi, M. H.; Ayaz, A. A. *Anal. Chem.* **1963**, *35*, 908.

(10) Simoyi, R. H. *Private communication*.

(11) Kern, D. M.; Kim, C. H. *J. Am. Chem. Soc.* **1965**, *87*, 5309.

(12) De Meeus, J.; Sigalla, J. *J. Chim. Phys. Phys.-Chim. Biol.* **1966**, *63*, 453.

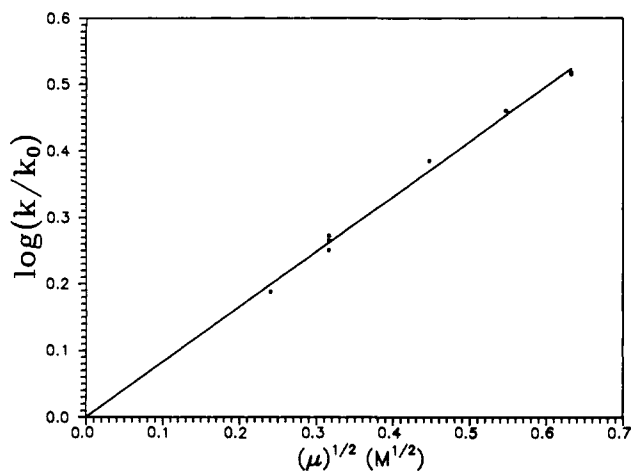


**Figure 2.** Ionic strength dependence, reaction S1:  $[I^-]_0 = [Br^{III}]_0 = 2.5 \times 10^{-4}$  M, pH 6, 0.05 M phosphate buffer.

The linearity of log-log plots shows no evidence of  $[I^-]$  inhibition on the rate of reaction, even though the  $[I^-]$  order is less than unity in the presence of phosphate buffer. With phthalate buffer the order is experimentally indistinguishable from unity. We conclude that the phosphate buffer reacts with some species and that the phthalate buffer reacts less or not at all. From these experiments, using only phthalate buffer, we find that reaction S1 has the simple rate equation

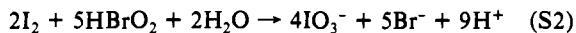
$$\frac{1}{2} \frac{d([I_2] + [I_3^-])}{dt} = k[BrO_2^-][I^-]a_{H^+} \quad (1)$$

where  $k = 2 \times 10^9 \text{ M}^{-2} \text{ s}^{-1}$  for  $\mu \sim 0.1$  M at 25 °C. This value of the rate constant is not very different from the previous value<sup>6</sup> of  $7.2 \times 10^8 \text{ M}^{-2} \text{ s}^{-1}$  for phthalate buffer and  $\mu = 0.2$  M. In selecting the value  $7.2 \times 10^8 \text{ M}^{-2} \text{ s}^{-1}$ , we have deleted the buffer-dependent term attributed by Ferranti and Indelli<sup>6</sup> to buffer catalysis, because we found no evidence for such an effect.

Changes in  $[H^+]$  change the ratio of buffer acid to its conjugate base. Contrary to the previous study,<sup>6</sup> we found no change in rate constant attributable to changes in this ratio.

We carried out some experiments at constant concentration of  $Br^{III}$ ,  $I^-$ ,  $H^+$ , and buffer but with varying ionic strength. We found an increase in rate constant with increasing ionic strength, which is opposite to the trend previously reported.<sup>6</sup> We plotted  $\log(k/k_0)$  against  $\mu^{1/2}$  (Figure 2), where  $k_0$  is the zero ionic strength rate constant calculated by extrapolation of the data to this point, and found a straight line with regression slope  $0.83 \pm 0.03$ .<sup>13</sup>

**Production of Iodate.** If  $Br(III)$  is not totally consumed by reaction S1, the iodine formed is consumed relatively rapidly through reaction S2. This reaction, combined with reaction S1,



yields reaction S3, the overall reaction in excess  $Br(III)$ .

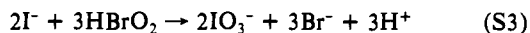
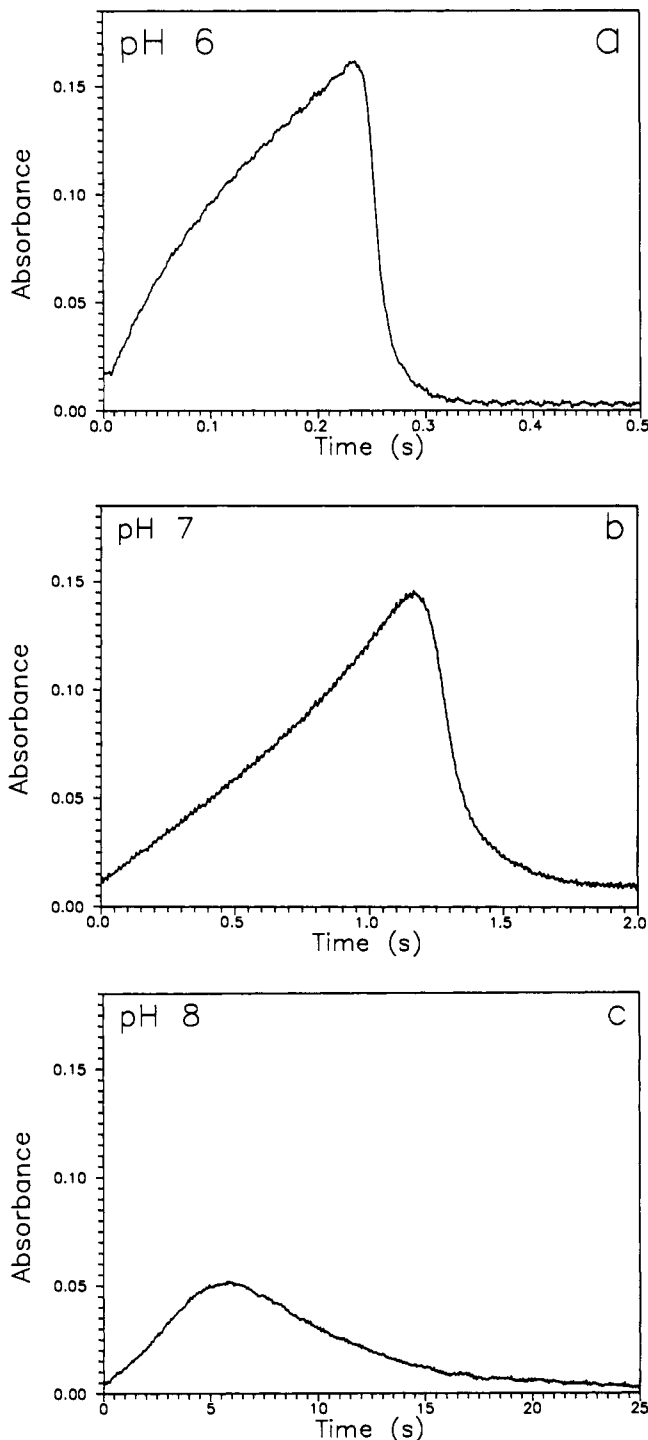


Figure 3a–c shows representative optical absorbance–time curves obtained for clock reaction behavior in the closed system  $Br^{III}/I^-$  as a function of pH in the range 6–8. This clock reaction has not been previously observed, because earlier studies of the  $Br^{III}/I^-$  system were carried out under conditions of excess  $[I^-]_0$ .

Reaction S2 is manifested shortly before reaction S1 terminates. At pH 6 (Figure 4), for example, total iodine(0) absorbance at 470 nm increases steadily during the first 0.26 s of the reaction, while iodide is consumed. At first,  $I_3^-$  absorbance at 350 nm increases, because of increasing concentration of iodine in a solution that still contains plentiful iodide. However, after approximately 0.1 s, the 350-nm absorbance begins to decrease, because the falling iodide concentration shifts the equilibrium between  $I_2$  and  $I_3^-$  in the direction of  $I_2$ . When almost all iodide



**Figure 3.** Stopped-flow absorbance results at pH 6 (a), 7 (b), and 8 (c):  $\lambda = 470$  nm; 0.05 M phosphate buffer;  $\mu = 0.06$  M;  $[Br^{III}]_0 = 8.6 \times 10^{-4}$  M;  $[I^-]_0 = 5 \times 10^{-4}$  M.

is consumed (vertical dashed line) and the absorbance at 350 nm is very low reaction S2 starts. (Note that for iodine at 470 nm  $\epsilon = 740 \text{ M}^{-1} \text{ cm}^{-1}$  and for  $I_3^-$  at 350 nm  $\epsilon = 27 \times 10^3 \text{ M}^{-1} \text{ cm}^{-1}$ .<sup>14</sup>)

To determine the range of concentrations for which the clock event occurs, a series of experiments was performed in which the ratio  $R = [Br^{III}]_0/[I^-]_0$  was varied. We found that if  $R < 1/4$  no clock event is observed. In the range  $1/4 < R < 3/2$ , the primary clock event is followed by a secondary increase in absorbance (Figure 5). For  $R \geq 3/2$  no secondary increase is observed (bottom curve in Figure 5). Therefore, the clock event

(13) Atkins, P. W. *Physical Chemistry*, 4th ed.; W. H. Freeman and Company: New York, 1990; p 861.

(14) Troy, R. C.; Kelley, M. D.; Nagy, J. C.; Margerum, D. W. *Inorg. Chem.* **1991**, *30*, 4838.

Table II. Reaction Mechanism and Forward and Reverse Rate Constants

		Reactions of HBrO <sub>2</sub>	
R1	HBrO <sub>2</sub> ⇌ BrO <sub>2</sub> <sup>-</sup> + H <sup>+</sup>	3.73 × 10 <sup>6</sup> s <sup>-1</sup>	1 × 10 <sup>10</sup> M <sup>-1</sup> s <sup>-1</sup>
R2	HBrO <sub>2</sub> + I <sup>-</sup> → HOI + BrO <sup>-</sup>	7.46 × 10 <sup>5</sup> M <sup>-1</sup> s <sup>-1</sup>	
R3	HBrO <sub>2</sub> + HOI → HOBr + HIO <sub>2</sub>	6 × 10 <sup>7</sup> M <sup>-1</sup> s <sup>-1</sup>	
		Some HOBr Reactions	
R4	HOBr + HOI → Br <sup>-</sup> + HIO <sub>2</sub> + H <sup>+</sup>	1 × 10 <sup>6</sup> M <sup>-1</sup> s <sup>-1</sup>	
R5	HOBr + HIO <sub>2</sub> → Br <sup>-</sup> + IO <sub>3</sub> <sup>-</sup> + 2H <sup>+</sup>	1 × 10 <sup>6</sup> M <sup>-1</sup> s <sup>-1</sup>	
R6	HOBr ⇌ H <sup>+</sup> + BrO <sup>-</sup>	15.8 s <sup>-1</sup>	1 × 10 <sup>10</sup> M <sup>-1</sup> s <sup>-1</sup>
		Some HIO <sub>2</sub> Reactions	
R7	HIO <sub>2</sub> + I <sup>-</sup> → HOI + IO <sup>-</sup> (→ HOI)	2 × 10 <sup>5</sup> M <sup>-1</sup> s <sup>-1</sup>	
R8	HIO <sub>2</sub> + HOI → IO <sub>3</sub> <sup>-</sup> + I <sup>-</sup> + 2H <sup>+</sup>	6 × 10 <sup>3</sup> M <sup>-1</sup> s <sup>-1</sup>	
		Reactions with IBr	
R9	IBr + H <sub>2</sub> O → Br <sup>-</sup> + HOI + H <sup>+</sup>	8 × 10 <sup>5</sup> s <sup>-1</sup>	
R10	HOBr + I <sup>-</sup> → IBr + OH <sup>-</sup>	5 × 10 <sup>9</sup> M <sup>-1</sup> s <sup>-1</sup>	
R11	HOBr + I <sub>2</sub> → IBr + HOI	1 × 10 <sup>7</sup> M <sup>-1</sup> s <sup>-1</sup>	
R12	IBr + I <sup>-</sup> → I <sub>2</sub> + Br <sup>-</sup>	2 × 10 <sup>9</sup> M <sup>-1</sup> s <sup>-1</sup>	
		Iodine Hydrolysis	
R13	I <sub>2</sub> + OH <sup>-</sup> ⇌ I <sub>2</sub> OH <sup>-</sup>	1 × 10 <sup>10</sup> M <sup>-1</sup> s <sup>-1</sup>	6 × 10 <sup>5</sup> s <sup>-1</sup>
R14	I <sub>2</sub> OH <sup>-</sup> ⇌ HOI + I <sup>-</sup>	6 × 10 <sup>3</sup> s <sup>-1</sup>	2.5 × 10 <sup>6</sup> M <sup>-1</sup> s <sup>-1</sup>
		Water Equilibrium	
R15	H <sub>2</sub> O ⇌ H <sup>+</sup> + OH <sup>-</sup>		
	(μ = 0.06 M)	3.6 × 10 <sup>-5</sup> s <sup>-1</sup>	1.3 × 10 <sup>11</sup> M <sup>-1</sup> s <sup>-1</sup>
	(μ = 0.10 M)	3.90 × 10 <sup>-5</sup> s <sup>-1</sup>	1.3 × 10 <sup>11</sup> M <sup>-1</sup> s <sup>-1</sup>

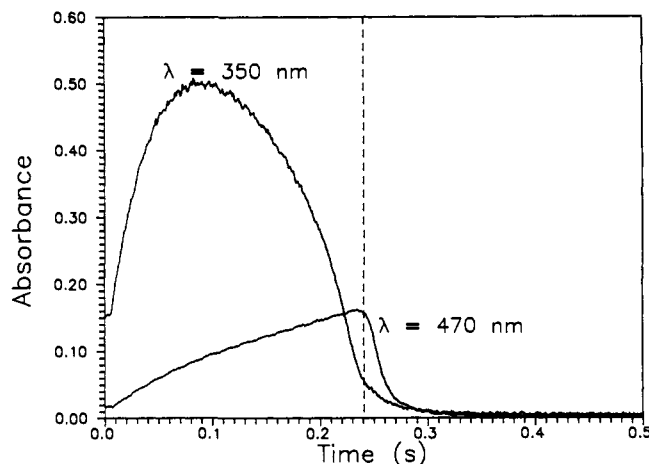


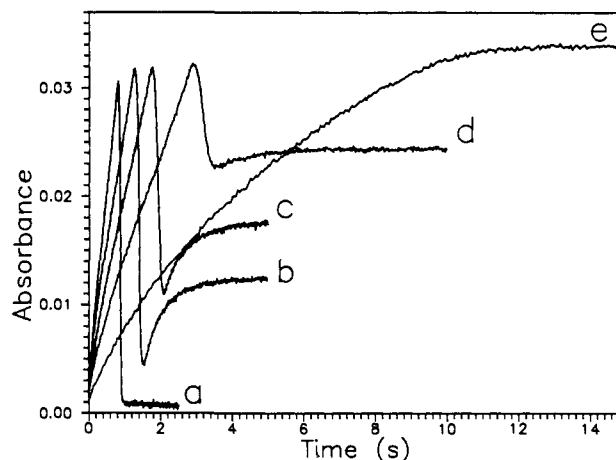
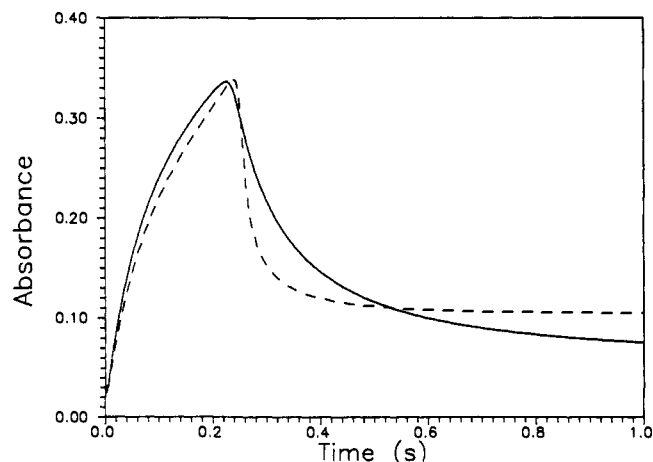
Figure 4. Comparison of kinetics curves at two wavelengths: same conditions as in Figure 3a.

occurs only in stoichiometric excess of Br(III) with respect to S1; experimentally, we find that above  $R = 3/2$  we cannot detect any iodine after the reaction is over, i.e., if there is a stoichiometric excess with respect to S3, all the I<sub>2</sub> is consumed by S2.

Initial addition of 10<sup>-3</sup> M bromide (Figure 6) does not significantly change the initial velocity of formation of iodine, but it suppresses the secondary increase in [I<sub>2</sub>] after the clock event. At the higher concentration 10<sup>-2</sup> M, bromide ion can make the clock event less abrupt.

#### Mechanism and Computer Simulation

In developing this mechanism (Table II), our starting point was the mechanism successfully used to model the oscillating bromate-iodide reaction.<sup>15</sup> In addition to the batch reaction described herein, the set of reactions presented in Table II can model the recently discovered bromite-iodide system that oscillates in an open, flow-through reactor in the absence of buffer.<sup>16</sup> This set of reactions is a subset of a more complete mechanism that can describe both systems: bromite-iodide and bromate-iodide, in both closed (clock reaction) and open (oscillations) reactors; modeling of several bromine-based oscillators and the larger mechanism will be described in a later paper.<sup>17</sup>

Figure 5. Effect of changing  $R$  on the secondary I<sub>2</sub> peak: pH 5.7, 0.05 M phthalate buffer, μ = 0.1 M, [I<sup>-</sup>] = 1.0 × 10<sup>-4</sup> M; [Br<sup>III</sup>]<sub>0</sub> = 1.5 × 10<sup>-4</sup> M (a), 1.0 × 10<sup>-4</sup> M (b), 7.5 × 10<sup>-5</sup> M (c), 5.0 × 10<sup>-5</sup> M (d), 2.5 × 10<sup>-5</sup> M (e).Figure 6. Effect of initially added Br<sup>-</sup> on the kinetics curve: pH 6, 0.05 M phosphate buffer, μ = 0.1 M, [Br<sup>III</sup>]<sub>0</sub> = 1.0 × 10<sup>-3</sup> M, [I<sup>-</sup>]<sub>0</sub> = 1.0 × 10<sup>-3</sup> M; (---) [Br<sup>-</sup>]<sub>0</sub> = 1.0 × 10<sup>-3</sup> M, (—) [Br<sup>-</sup>] = 1.0 × 10<sup>-2</sup> M.(15) Citri, O.; Epstein, I. R. *J. Am. Chem. Soc.* **1986**, *108*, 357.(16) Orbán, M.; Epstein, I. R. *J. Am. Chem. Soc.* **1992**, *114*, 1252.

(17) Faria, R. B.; Lengyel, I.; Epstein, I. R.; Kustin, K. In preparation.

The standard free energies of formation  $\Delta G_f^\circ$  for all species in Table II are well-known quantities, except for that of HIO<sub>2</sub>.

Using a  $\Delta G_f^\circ(\text{HIO}_2)$  value of  $-69 \text{ kJ mol}^{-1}$ ,<sup>18</sup> we calculate that, except for reactions R4 and R9, all reactions in Table II are strongly favored thermodynamically at pH 0. At pH 7, however, all reactions, including reactions R4 and R9, are thermodynamically favored, a trend that continues to higher pH. The least favorable reaction, R9, has an apparent equilibrium constant of 2 at a fixed pH of 7. Calculations with the reverse of reaction R9 included in the mechanism gave results identical with those for which this step was excluded, and it was dropped for the sake of simplicity.

Reactions involving  $\text{Br}_2$  and  $\text{I}_3^-$ , needed for a fuller description of a greater number of mechanistic possibilities, were included at first, but their elimination does not change the results, and they were omitted to keep the calculations as simple as possible. The following considerations indicate that this omission is readily justified. In the case of  $\text{Br}_2$ , it is important to note that we are modeling reactions in the pH range 6–8 where  $\text{Br}_2$  is insignificant. Moreover, we did not detect formation of  $\text{Br}_2$  in our batch experiments. For  $\text{I}_3^-$ , the equilibrium between this species and  $\text{I}_2$  is very rapidly established, and reactions with  $\text{I}_2$  are important only when the iodide is in very low concentration, i.e., when high concentrations of  $\text{I}_3^-$  are not present. Other species, such as  $\text{I}_2\text{Br}^-$  and  $\text{IBr}_2^-$ , were considered, but these were discarded after calculations showed that their presence was ineffective. Two intermediate species,  $\text{I}_2\text{OH}^-$  and  $\text{IBr}$ , are required for successful simulation of the experimental data.<sup>14,19</sup>

Acid–base equilibria play an important role in the mechanism, principally because  $\text{HBrO}_2$  and  $\text{HOBr}$  are assumed to be the only reactive Br(III) and Br(I) species in our mechanistic scheme. The value for the  $\text{p}K_a$  of  $\text{HBrO}_2$ , reaction R1, that we have used departs from previous values. Two such earlier quantities are 6.3 and 4.9, derived from studies of the decomposition of bromite solutions at near neutral pH and 1 M  $\text{H}_2\text{SO}_4$ , respectively.<sup>20,21</sup> We use  $\text{p}K_a = 3.43$  ( $K_a = 3.73 \times 10^{-4} \text{ M}$ ), which we obtained experimentally, in an independent investigation, by measuring the initial velocity of the reaction between Br(III) and  $\text{I}^-$  in the pH range 3–6,  $\mu = 0.06 \text{ M}$ .<sup>22</sup> A lower  $\text{p}K_a$  for  $\text{HBrO}_2$  makes it unnecessary to consider the disproportionation of  $\text{HBrO}_2$  in the pH range 6–8, because this reaction is slow compared with the clock reaction. In addition,  $\text{HBrO}_2$  disproportionation kinetics had no discernible impact on the simulation when it was included in the mechanism. For the reverse of reaction R1, we use the diffusion-limited rate constant for reactions in liquid water.<sup>23</sup>

Other acid–base equilibria are reaction R6, for which we use a  $\text{p}K_a$  for  $\text{HOBr}$  equal to 8.8,<sup>24</sup> and reaction R15, for which we use the experimental value from Eigen and de Maeyer for the reverse reaction<sup>25</sup> and calculate the rate constant for the forward reaction from the appropriate  $\text{p}K_w$  for the value of  $\mu$  used in the experiments we are modeling, i.e.,  $\text{p}K_w = 13.811$  for  $\mu = 0.06 \text{ M}$  and  $\text{p}K_w = 13.781$  for  $\mu = 0.1 \text{ M}$ .<sup>26</sup>

The following describes the remaining reactions and rate constants used in the simulation and gives reasons for their selection.

**Reaction R2:** From our  $\text{p}K_a$  value,  $\text{BrO}_2^-$  is the dominant Br(III) species in the pH range studied. To obtain the rate constant for reaction R2, we multiply our value for the third-order rate constant,  $2 \times 10^9 \text{ M}^{-2} \text{ s}^{-1}$ , by the equilibrium constant for dissociation of  $\text{HBrO}_2$ ,  $3.73 \times 10^{-4} \text{ M}$ .

**Reaction R3:** A range of values has been used to model bromate–iodide and bromate–chlorite–iodide oscillating systems:<sup>15,27</sup>  $1 \times 10^9$  and  $2 \times 10^7 \text{ M}^{-1} \text{ s}^{-1}$ . The experimental value for this

reaction with  $\text{HClO}_2$  is  $6 \times 10^7 \text{ M}^{-1} \text{ s}^{-1}$ ,<sup>11</sup> which is the value we use for reaction R3. Calculating our  $\text{p}K_a$  for  $\text{HBrO}_2$  at zero ionic strength gives 3.58.<sup>22</sup> Using this value together with  $\Delta G_f^\circ(\text{BrO}_2^-) = 27.2 \text{ kJ mol}^{-1}$ ,<sup>15</sup> we calculate a  $\Delta G_f^\circ(\text{HBrO}_2)$  value of  $6.5 \text{ kJ mol}^{-1}$ , which is close to  $\Delta G_f^\circ(\text{HClO}_2)$  ( $5.9 \text{ kJ mol}^{-1}$ ). The values for  $\Delta G_f^\circ(\text{HOCl})$  ( $-79.9 \text{ kJ mol}^{-1}$ )<sup>28</sup> and  $\Delta G_f^\circ(\text{HOBr})$  ( $-82.4 \text{ kJ mol}^{-1}$ )<sup>29</sup> are also close together, which suggests that the correct value for reaction R3 should not be far from  $6 \times 10^7 \text{ M}^{-1} \text{ s}^{-1}$ . Therefore, we are using a value close to that determined for a homologous reaction in which the reactive species is  $\text{HClO}_2$  and not  $\text{ClO}_2^-$ , which supports our choice of  $\text{HBrO}_2$  and not  $\text{BrO}_2^-$  as the reactive species.

**Reaction R4:** The spread of values for the rate constant of this step used in modeling bromate–iodide and bromate–chlorite–iodide oscillating systems is not wide:  $2 \times 10^8$  and  $1 \times 10^8 \text{ M}^{-1} \text{ s}^{-1}$ .<sup>15,27</sup> These values are for the analogous reaction  $\text{HOCl} + \text{HOI} \rightarrow \text{Cl}^- + \text{HIO}_2 + \text{H}^+$ . We could not use a value as high as  $10^8 \text{ M}^{-1} \text{ s}^{-1}$  for reaction R4 because this choice makes the clock event less abrupt and kills the secondary iodine increase, making the calculated kinetics curve similar to that at higher  $[\text{Br}^-]$  (Figure 6). Indeed, if the rate constants follow the thermodynamic trend,  $\Delta G_f^\circ(\text{Cl}^-)$  ( $-131.0563 \text{ kJ mol}^{-1}$ )<sup>28</sup> being significantly more negative than  $\Delta G_f^\circ(\text{Br}^-)$  ( $-103.97 \text{ kJ mol}^{-1}$ )<sup>29</sup> then a value lower than  $10^8 \text{ M}^{-1} \text{ s}^{-1}$  makes sense.

**Reaction R5:** This value was taken from the literature.<sup>27</sup>

**Reaction R7:** Previously, this reaction, studied in very acidic media, has been associated with an  $\text{H}^+$  dependence,<sup>27,30–34</sup> but this  $\text{H}^+$  dependence in our model causes the clock event at pH 7 and 8 to occur too late compared with experiment. There is no experimental evidence supporting this effect, however, and Furrow was able to model  $\text{I}_2$  reactions involving reaction R7 without an  $\text{H}^+$  dependence.<sup>35</sup> We have followed Furrow's practice and have removed this  $\text{H}^+$  dependence. In so doing, we obtain the correct time scale for all changes in pH.

**Reaction R8:** The reported values for this reaction are 130,<sup>30</sup> 230,<sup>32,35</sup> 167,<sup>36</sup> and  $1.0 \times 10^5 \text{ M}^{-1} \text{ s}^{-1}$  (40 °C, claimed to be a better choice at higher  $[\text{I}^-]$ );<sup>37</sup> the value we use is within this range.

**Reactions R9 and R10:** We use experimentally determined values.<sup>14</sup>

**Reaction R11:** Our value lies between the values used to model the oscillating systems  $\text{BrO}_3^- - \text{I}^-$  ( $8 \times 10^7 \text{ M}^{-1} \text{ s}^{-1}$ )<sup>15</sup> and  $\text{BrO}_3^- - \text{ClO}_2^- - \text{I}^-$  ( $5 \times 10^6 \text{ M}^{-1} \text{ s}^{-1}$ ).<sup>27</sup>

**Reaction R12:** We use the experimental value<sup>14</sup> for the reaction  $\text{IBr} + \text{I}^- \rightarrow \text{I}_2\text{Br}^-$ . As this last species decomposes to  $\text{I}_2 + \text{Br}^-$ , use of the overall reaction reduces by one the number of species in the model.

**Reaction R13:** We used the experimental values determined by temperature-jump spectrometry at 20 °C.<sup>19</sup>

**Reaction R14:** Our value lies between the two known experimental values (forward reaction R15,  $3 \times 10^7$  and  $994 \text{ s}^{-1}$ ; reverse reaction R14,  $3.2 \times 10^5$  and  $5 \times 10^5 \text{ M}^{-1} \text{ s}^{-1}$ ).<sup>19,38</sup> Difficulties in using the low values of Palmer and van Eldik,<sup>38</sup> in modeling studies, have been noticed before,<sup>35</sup> and the higher values of Eigen and Kustin<sup>19</sup> were also unsatisfactory in our model. Moreover, taking  $K_w$  at 25 °C and  $\mu = 0.06 \text{ M}$  (see Table II), and using our values for reaction R14, we find  $K_{\text{eq}} = 6.2 \times 10^{-13} \text{ M}^2$  for the  $\text{I}_2$

(18) Sharma, K. R.; Noyes, R. M. *J. Am. Chem. Soc.* **1976**, *98*, 4345.

(19) Eigen, M.; Kustin, K. *J. Am. Chem. Soc.* **1962**, *84*, 1355.

(20) Massagli, A.; Indelli, A.; Pergola, F. *Inorg. Chim. Acta* **1970**, *4*, 593.

(21) Field, R. J.; Försterling, H.-D. *J. Phys. Chem.* **1986**, *90*, 5400.

(22) Faria, R. B.; Epstein, I. R.; Kustin, K. *J. Phys. Chem.*, in press.

(23) Jordan, P. *Chemical Kinetics and Transport*; Plenum Press: New York, 1979; p 138.

(24) Troy, R. C.; Margerum, D. W. *Inorg. Chem.* **1991**, *30*, 3538.

(25) Eigen, M.; de Maeyer, L. Z. *Elektrochem.* **1955**, *59*, 986.

(26) Sweeton, F. H.; Mesmer, R. E.; Baes, C. F., Jr. *J. Solution Chem.* **1974**, *3*, 191.

(27) Citri, O.; Epstein, I. R. *J. Phys. Chem.* **1988**, *92*, 1865.

(28) Mussini, T.; Longhi, P. In *Standard Potentials in Aqueous Solution*; Bard, A. J., Parsons, R., Jordan, J., Eds.; Marcel Dekker, Inc.: New York, 1985; p 70.

(29) Mussini, T.; Longhi, P. In *Standard Potentials in Aqueous Solution*; Bard, A. J., Parsons, R., Jordan, J., Eds.; Marcel Dekker, Inc.: New York, 1985; p 78.

(30) Noszticzus, Z.; Noszticzus, E.; Schelly, Z. A. *J. Phys. Chem.* **1983**, *87*, 510.

(31) Epstein, I. R.; Kustin, K. *J. Phys. Chem.* **1985**, *89*, 2275.

(32) Citri, O.; Epstein, I. R. *J. Phys. Chem.* **1987**, *91*, 6034.

(33) Luo, Y.; Epstein, I. R. *J. Phys. Chem.* **1989**, *93*, 1398.

(34) Simoyi, R. H.; Manyonda, M.; Masere, J.; Mtambo, M.; Ncube, I.; Patel, H.; Epstein, I. R.; Kustin, K. *J. Phys. Chem.* **1991**, *95*, 770.

(35) Furrow, S. *J. Phys. Chem.* **1987**, *91*, 6034.

(36) Liebhafsky, H. A.; Roe, G. M. *Int. J. Chem. Kinet.* **1979**, *11*, 693.

(37) Edblom, E. C.; Gyorgy, L.; Orbán, M.; Epstein, I. R. *J. Am. Chem. Soc.* **1987**, *109*, 4876.

(38) Palmer, D. A.; van Eldik, R. *Inorg. Chem.* **1986**, *25*, 928.

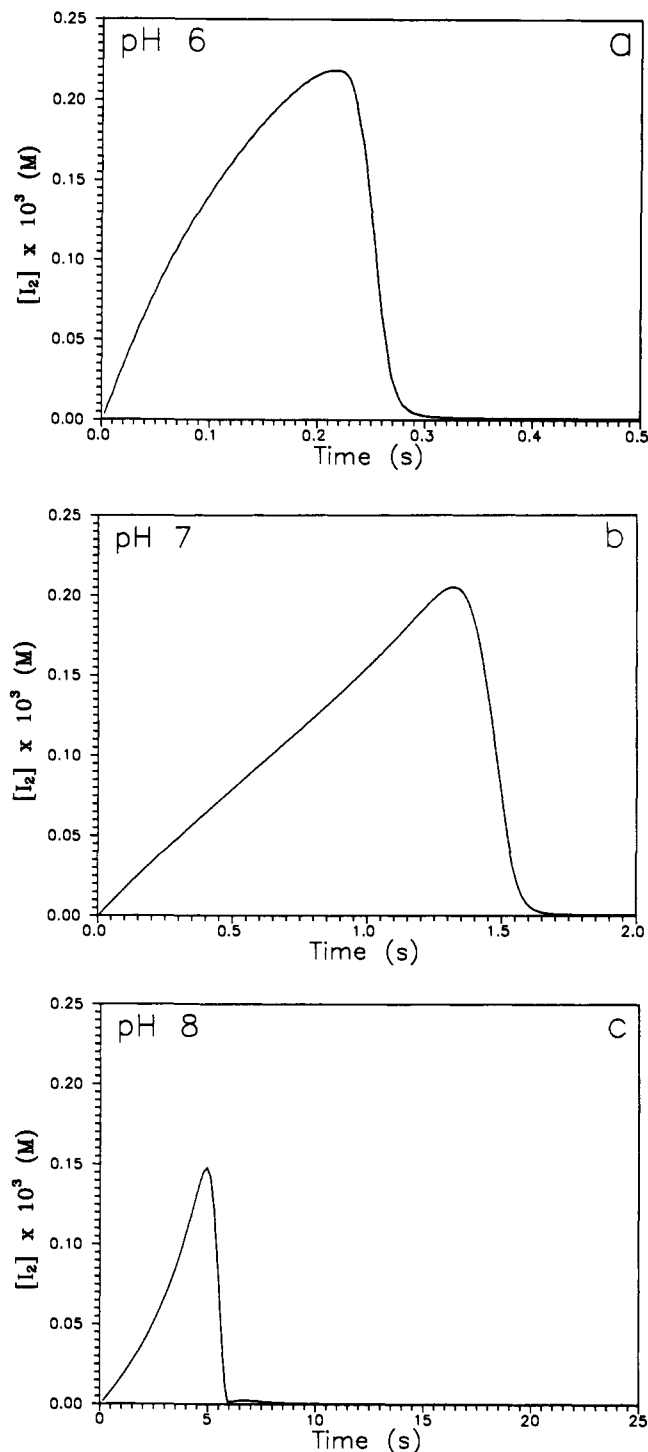


Figure 7. Computer simulation of kinetics curves; conditions identical with those of Figure 3; ordinate scale identical with that of Figure 3 for ease of comparison: (a) pH 6, (b) pH 7, (c) pH 8.

+  $\text{H}_2\text{O} \rightleftharpoons \text{HOI} + \text{I}^- + \text{H}^+$  reaction, which is quite close to  $3.13 \times 10^{-13} \text{ M}^2$  at  $20^\circ \text{C}$  and  $\mu \sim 0 \text{ M}$ , obtained by averaging literature values,<sup>39</sup> and almost the same as the  $5.44 \times 10^{-13} \text{ M}^2$  used to model the Dushman reaction.<sup>36</sup> Our model is highly sensitive to the values of reactions R13 and R14. Changes of  $\pm 10\%$  in the rate constants for these reactions produce significant changes in dynamical characteristics such as time scale, curve shape, and maximum amount of iodine formed.

The  $[\text{I}_2]$ -time curves calculated from the mechanism in Table II are shown in Figures 7a-c and 8 and should be compared with Figures 3a-c and 5. The calculations were performed on a 386/25

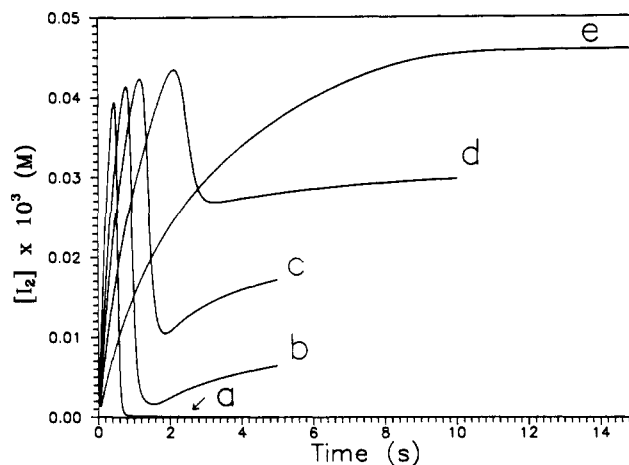


Figure 8. Computer simulation of kinetics curves; conditions identical with those of Figure 5; ordinate scale identical with that of Figure 5 for ease of comparison.

MHz PC-compatible microcomputer using a program written in Turbo Pascal that solves autonomous ordinary differential equation systems by a semi-implicit Runge-Kutta method.<sup>40</sup>

The agreement with experimental results is generally excellent. In the pH range 6-8 our model predicts the correct time scale and the decrease in maximum total amount of iodine formed as pH increases. The appearance of the curves is quite similar to experiment at pH 6 and 7, but at pH 8 the decay of iodine concentration in the simulation is faster than in the experiment. We have made many changes in our model in attempts to model this curve at pH 8 more accurately, but with no success.

#### Discussion

The mechanism presented here encompasses broader dynamics than a single reaction such as reaction R1 or a clock reaction. It can be applied both to the clock reaction exhibited in near neutral pH in a closed reactor and to the oscillating reaction exhibited in acidic pH in an open reactor. Throughout the pH region where clock reaction behavior is exhibited,  $\text{BrO}_2^-$  is the dominant Br(III) species. To explain the clock reaction over its entire pH range and the oscillating reaction over a lower pH range, we use a model based on reactive  $\text{HBrO}_2$  ( $\text{p}K_a = 3.43$ , obtained through a separate set of experiments)<sup>22</sup> and relatively unreactive  $\text{BrO}_2^-$ . In the mechanism of the clock reaction, only two reactions, R2 and R3, involve Br(III). Of these, the rate constant for reaction R2 is based on our experimental values of the third-order rate constant; and the rate constant for reaction R3 is one used in a study modeling reactions in acidic media where  $\text{HBrO}_2$  is the predominant Br(III) species,<sup>11</sup> and for which the assignment of rate constant with species is unambiguous. Using  $\text{BrO}_2^-$  as a reactive species has two major drawbacks: (1) the pH dependence of the clock reaction line shape simulation worsens and (2) the pH dependence of the clock reaction time scale actually goes in the wrong direction, becoming shorter at higher pH, contrary to experimental results. Therefore, only  $\text{HBrO}_2$  is considered the reactive Br(III) species in our mechanism.

Two aspects of the dynamics remain unexplained, however. In our rederivation of the rate law for reaction S1, we found two significant changes: a lack of general acid catalysis and a positive ionic strength dependence. Even if we correct the pH values for different  $\mu$  by use of the Davies equation,<sup>41</sup> coupled with the Henderson-Hasselbach equation, or even without neglecting any protolytic species arising from buffer equilibria,<sup>42</sup> we obtain a positive slope with a value close to 1.<sup>13</sup> We were also unable to model the  $[\text{Br}^-]$  dependence (Figure 6). Indeed,  $\text{Br}^-$  is not a

(40) Kaps, P.; Rentrop, P. *Numer. Math.* 1979, 33, 55.

(41) Meites, L. *Handbook of Analytical Chemistry*; McGraw-Hill: New York, 1963; p 18.

(42) Gordus, A. A. *J. Chem. Educ.* 1991, 68, 215.

(39) Palmer, D. A.; Lietzke, M. H. *Radiochim. Acta* 1982, 31, 37.

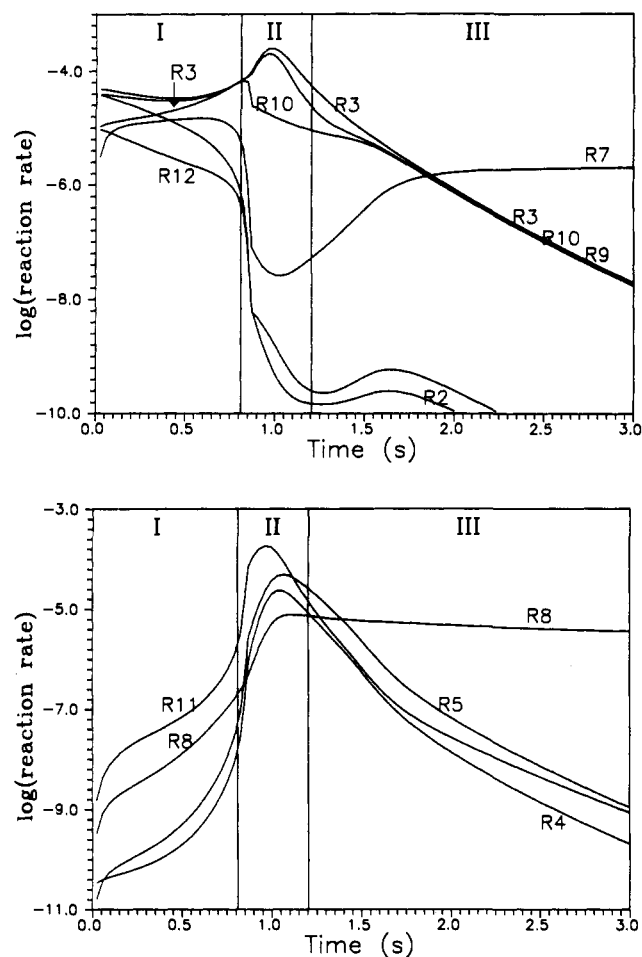


**Figure 9.** Logarithm of calculated reaction rates in regions I, II, and III for selected individual steps in the reaction mechanism; conditions identical with Figure 5b: (a, top) reactions R2, R3, R7, R9, R10, R12; (b, bottom) reactions R4, R5, R8, R11.

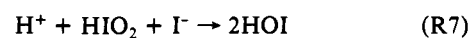
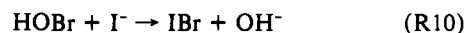
reactant in our mechanism (Table I). We have attempted to include reactions with  $\text{Br}^-$  as a reagent, but none of these reactions could account for the experimentally observed behavior. As expected,  $\text{Br}^-$  behaves as an unreactive final product of the last stages of the reduction of  $\text{Br(III)}$  in the pH range 6–8.

The clock reaction experimental curves show three separate regions of change in  $[\text{I}_2]$ : (I) increase, (II) fast decrease, and (III) small secondary increase. These three regions can be explained by comparing, at the boundaries between regions, reaction velocities calculated from our mechanism. The computer program calculates the concentration of each species during the course of the reaction and, therefore, the velocity of each reaction (Figure 9a,b), which aids this comparison.

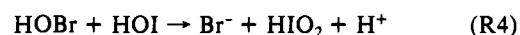
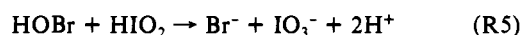
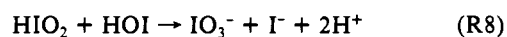
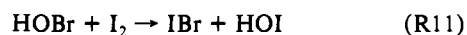
For region I (increasing  $[\text{I}_2]$ ), the most important reactions are R2, R3, R7, R9, R10, and R12 (Figure 9a). Reactions R2 and R12 decrease in importance as the clock event starts (vertical line between regions I and II); all other reactions from this group of six reactions increase in value. Trends in the rates of reactions R2 and R3 are opposite: that for reaction R2 decreases and that for reaction R3 increases. The rates cross halfway through region I, showing that reaction R3 is an important pathway for  $\text{HBrO}_2$  consumption. In the same fashion,  $\text{I}^-$  reacts at very high speed, not only with  $\text{HBrO}_2$  but also with  $\text{HOBr}$  (R10),  $\text{HIO}_2$  (R7), and  $\text{IBr}$  (R12).

Of course, reactions R13 and R14 (not shown in Figure 9) operate at very high speeds throughout this region to form  $\text{I}_2$  from  $\text{HOI}$  and  $\text{I}^-$ , or to reverse this reaction when  $[\text{I}^-]$  is very low.

As we note from Figure 3, the shapes of absorbance–time curves are quite different for pH 6 and 7. In explaining this difference we consider two subsets of reactions at the end of region I, in order of decreasing reaction velocity (Figure 9a)



and (Figure 9b)



When conditions change from pH 6 to 7, differences in rates that change the shape of the kinetics curve occur at the end of region I: (1) reaction R7 increases in importance, becoming close to reaction R3; (2) reaction R8 gets closer to reaction R11 (this reaction becomes even more important than reaction R11 at pH 8); (3) reactions R5 and R4 decrease even more in importance relative to reactions R8 and R11.

From (1) we conclude that the autocatalytic route including reactions R3 + R7 is more active at pH 7 than at pH 6, relative to the other reactions. This conclusion can be explained by higher  $[\text{HIO}_2]$  and  $[\text{HOI}]$ . Statement (2) confirms this conclusion. From (3) we see that reactions of  $\text{HOBr}$  decline in importance at higher pH, not because of the  $\text{p}K_a$  of  $\text{HOBr}$ , which is too high to play such a role, but because  $[\text{HOBr}]$  has declined.

Why should there be more  $\text{HIO}_2$  and  $\text{HOI}$  and less  $\text{HOBr}$  at higher pH? The concentrations of these species depend critically on the equilibrium constant for dissociation of  $\text{HBrO}_2$ . Our relatively lower  $\text{p}K_a$  for  $\text{HBrO}_2$  produces exactly the right decrease in  $[\text{HBrO}_2]$  at pH 7 compared with pH 6, to help account for the clock reaction time scale dependence on pH with reasonable accuracy. In addition, the lower  $[\text{HBrO}_2]$  at higher pH will slow down the formation of  $\text{HOBr}$  (by reactions R3 and R2), and reactions R10 and R9, which do not depend on pH, convert almost all  $\text{HOBr}$  formed to  $\text{Br}^-$ . At the same time, the sequence of reactions R10 + R9 makes  $\text{HOI}$ , which eventually yields  $\text{HIO}_2$  and more  $\text{HOI}$  by reactions R3 and R7.

Otherwise, lowering pH makes reactions R3 and R2 run at higher speeds, producing  $\text{HOBr}$  in such amounts that reaction R10 cannot destroy all of it at once. This change allows reactions R5 and R4 to destroy enough  $\text{HOI}$  and  $\text{HIO}_2$  to prevent the autocatalytic route of reactions R3 + R7 from running as fast as it does at higher pH.

The lower peak in  $[\text{I}_2]$  at higher pH is explained by the shift toward products in the iodine hydrolysis equilibrium as  $[\text{H}^+]$  decreases. In addition, at higher pH, lower  $[\text{HBrO}_2]$  causes lower  $[\text{HOBr}]$ , and this condition causes higher  $[\text{HOI}]$  and  $[\text{HIO}_2]$ , as explained above. Consequently, the increase in the rate of reaction R8 (see statement (2) above) pumps more iodine atoms into production of  $\text{IO}_3^-$ , and not as much  $\text{I}_2$  is formed at these higher pHs.

At the time of the peak in  $[\text{I}_2]$  (boundary between regions I and II), the solution is almost completely depleted of  $\text{I}^-$ ;  $[\text{HOBr}]$  is able to grow until reaction R11, the fastest reaction of the whole subset in region II, becomes important (Figure 9b, in which reaction R11 has an even higher rate than any reaction in Figure 9a). Therefore,  $\text{HOI}$  produced by reaction R11 cannot reform  $\text{I}_2$ , because there is no  $\text{I}^-$  remaining, consequently, the peak in  $\text{I}_2$  rapidly declines.

After the clock event, region III,  $\text{HBrO}_2$  is depleted. The most important reactions are R7 (Figure 9a) and R8 (Figure 9b), reforming  $\text{I}^-$  and  $\text{HOI}$ , a process that makes some  $\text{I}_2$ , and accounts for the third region of the overall reaction.

At pH 8, the mechanism does not model the clock reaction as well as it does at lower pH. This insufficiency may be due to a

lack of relevant data, such as a  $pK_a$  for  $\text{HIO}_2$ . The mechanism confirms, for the first time, a significant role for IBR in mixed oxyhalogen kinetics and augments the number of complex networks incorporating bromine(III) reactions for which a mechanistic explanation is available.

**Acknowledgment.** We thank Dr. István Lengyel for many

helpful discussions and for the use of his kinetic modeling program. This work was supported by Research Grant CHE-9023294 from the National Science Foundation and by Conselho Nacional de Desenvolvimento Científico e Tecnológico-CNPq (proc. 202081/90-7).

Registry No.  $\text{BrO}_2^-$ , 15477-77-7;  $\text{I}^-$ , 20461-54-5.

## Electronic Spectroscopy of Jet-Cooled Half-Sandwich Organometallic Complexes $\text{CaC}_5\text{H}_5$ , $\text{CaC}_5\text{H}_4\text{CH}_3$ , and $\text{CaC}_4\text{H}_4\text{N}$

Eric S. J. Robles,<sup>†</sup> Andrew M. Ellis,<sup>†</sup> and Terry A. Miller\*

Contribution from the Laser Spectroscopy Facility, Department of Chemistry, The Ohio State University, 120 West 18th Avenue, Columbus, Ohio 43210. Received March 10, 1992

**Abstract:** Laser excitation and dispersed fluorescence spectra of jet-cooled, open-faced organometallic complexes,  $\text{CaC}_5\text{H}_5$ ,  $\text{CaC}_5\text{H}_4\text{CH}_3$ , and  $\text{CaC}_4\text{H}_4\text{N}$ , are presented and analyzed. The electronic structure of these molecules can best be described as  $\text{Ca}^+$  being perturbed by  $\text{R}^-$  ( $\text{R} = \text{C}_5\text{H}_5$ ,  $\text{C}_5\text{H}_4\text{CH}_3$ , and  $\text{C}_4\text{H}_4\text{N}$ ). The electronic transitions observed here are essentially metal-centered. The electronic spectra of these complexes show extensive vibrational structure arising from excitation of skeletal and intra-ring modes. From this structure, we are able to determine the binding site of the metal atom, i.e., above the ring in a pentahapto ( $\eta^5$ ) bonding fashion. The electronic spectra of the fully-deuterated isotopomers  $\text{CaC}_5\text{D}_5$  and  $\text{CaC}_4\text{D}_4\text{N}$  are also presented here to provide information about "pure" hydrogenic vibrations in  $\text{CaC}_5\text{H}_5$  and  $\text{CaC}_4\text{H}_4\text{N}$ . Several vibronic bands of  $\text{CaC}_5\text{H}_5$  are also attributed to single quantum excitation of  $e_2$  modes, which indicates that this molecule is Jahn-Teller active in its  $\tilde{A}^2E_1$  electronic state. In the case of  $\text{CaC}_5\text{H}_4\text{CH}_3$ , methyl torsional bands are observed, from which the barrier to methyl free rotation and the change in conformation of the methyl group on  $\tilde{A}-\tilde{X}$  excitation are determined. This study represents the first spectroscopic study on  $\text{CaC}_5\text{H}_4\text{CH}_3$  in the gas phase.

### I. Introduction

The full-sandwich compound bis(cyclopentadienyl)calcium or calcocene,  $\text{Ca}(\text{C}_5\text{H}_5)_2$  (or  $\text{CaCp}_2$  for short), was synthesized first by Cotton and Wilkinson in 1954.<sup>1</sup> Since then  $\text{CaCp}_2$  and its ring-substituted derivatives have been structurally and spectroscopically characterized.<sup>2-7</sup> A single X-ray crystallographic diffraction study showed that  $\text{CaCp}_2$  (ref 4) has a polymeric structure in the solid state, in which four Cp rings are coordinated to each calcium atom in an  $\eta^1$ ,  $\eta^3$ ,  $\eta^5$ ,  $\eta^5$  fashion (the  $\eta^n$  notation means that there are  $n$  ligand atoms bonded to the metal). Unfortunately, because of the polymeric nature of solid  $\text{CaCp}_2$ , its volatility is extremely low, which prevented a molecular structure determination of this compound in the gas phase.<sup>5</sup> The only available gas-phase work on  $\text{CaCp}_2$  is a mass spectrometric study of this molecule, which showed that the most abundant molecular ions are  $\text{CaCp}_2^+$  and  $\text{CaCp}^+$ .<sup>4</sup> The low-volatility problem in polymeric  $\text{CaCp}_2$  was later resolved by completely substituting a methyl group for each of the five hydrogens in the Cp ring, to give the monomeric pentamethylcyclopentadienyl complex  $\text{Ca}(\text{C}_5\text{Me}_5)_2$ . A gas-phase electron diffraction study of  $\text{Ca}(\text{C}_5\text{Me}_5)_2$  revealed that the two  $\text{C}_5\text{Me}_5$  ligands are both  $\eta^5$ -bonded but are nonparallel, i.e.,  $\eta^5\text{-Ca}(\text{C}_5\text{Me}_5)_2$  is bent.<sup>7</sup> Ab initio calculations on  $\text{CaCp}_2$  were performed but failed to explain why  $\text{Ca}(\text{C}_5\text{Me}_5)_2$  has a bent structure and not the regular sandwich structure with parallel Cp rings.

Recently, Bernath and co-workers<sup>8,9</sup> reported laser spectroscopic studies on the half-sandwich complexes  $\text{CaCp}$  and  $\text{CaC}_4\text{H}_4\text{N}$  ( $\text{CaPy}$ ). Unlike the closed-shell species  $\text{CaCp}_2$ ,  $\text{CaCp}$  and  $\text{CaPy}$

are chemically unstable transient species, so-called organometallic free radicals. Bernath and co-workers prepared these molecules in the gas phase using the Broida oven technique, in which the metal (Ca) was evaporated from a resistively heated alumina crucible, after which the metal vapor is mixed with an appropriate oxidant gas under flowing conditions yielding the desired molecular species. In addition to  $\text{CaCp}$  and  $\text{CaPy}$ , a number of radicals of the type  $\text{M-R}$ , where M is an alkaline earth metal (Ca, Sr, Ba) and R is an organic ligand (e.g., methyl ( $\text{CH}_3$ ),<sup>10,11</sup> methoxy ( $\text{OCH}_3$ ),<sup>12,13</sup> Cp,<sup>8</sup> and Py<sup>9</sup>), have been studied.

A drawback of the Broida oven method is that molecules are produced with relatively high internal temperatures, 500 K being a typical rotational temperature. This results in substantial spectral congestion. For example, in a laser-induced fluorescence (LIF) study of  $\text{CaCp}^8$  and  $\text{CaC}_4\text{H}_4\text{N}$  ( $\text{CaPy}$ ),<sup>9</sup> the relatively high temperatures resulted in bands with full width at half-maximum (fwhm) of the order of  $50\text{ cm}^{-1}$ . With this resolution, closely

(1) Wilkinson, G.; Cotton, F. A. *Chem. Ind. (London)* **1954**, 11, 307.

(2) Fischer, E. O.; Stolzle, G. *Chem. Ber.* **1961**, 94, 2187.

(3) Allan, K. A.; Gowenlock, B. G.; Lindsell, W. E. *J. Organomet. Chem.* **1973**, 55, 229.

(4) Zenger, R.; Stucky, G. *J. Organomet. Chem.* **1974**, 80, 7.

(5) Blom, R.; Faegri, K., Jr.; Volden, H. V. *Organometallics* **1990**, 9, 372.

(6) Gardiner, M. G.; Raston, C. L.; Kennard, C. H. L. *Organometallics* **1991**, 10, 3680.

(7) Andersen, R. A.; Boncella, J. M.; Burns, C. J.; Blom, R.; Haaland, A.; Volden, H. V. *J. Organomet. Chem.* **1986**, 312, C49.

(8) O'Brien, L. C.; Bernath, P. F. *J. Am. Chem. Soc.* **1986**, 108, 5017.

(9) Bopeggera, A. M. R. P.; Fernando, W. T. M. L.; Bernath, P. F. *J. Phys. Chem.* **1990**, 94, 4476.

(10) Brazier, C. R.; Bernath, P. F. *J. Chem. Phys.* **1987**, 86, 5918.

(11) Brazier, C. R.; Bernath, P. F. *J. Chem. Phys.* **1989**, 91, 4548.

(12) Brazier, C. R.; Ellingboe, L. C.; Kinsey-Nielson, S.; Bernath, P. F. *J. Am. Chem. Soc.* **1986**, 108, 2126.

(13) O'Brien, L. C.; Brazier, C. R.; Bernath, P. F. *J. Mol. Spectrosc.* **1988**, 130, 33.

\* Corresponding author.

<sup>†</sup> 1991 Rohm and Haas and 1992 Phillips Petroleum Fellow.

<sup>†</sup> NATO/SERC and Ohio State Postdoctoral Fellow. Present address: Department of Chemistry, University of Leicester, University Road, Leicester LE1 7RH, England.